# UV Absorption Cross Sections of ClOOCl Are Consistent with Ozone Degradation Models

Hsueh-Ying Chen *et al.*

*Science* **324**, 781 (2009);
DOI: 10.1126/science.1171305

of the residual SST trends are statistically significant at the 95% level (*23*). Note that our analysis does not show that aerosols explain year-to-year changes in SST, but that their effect is realized when considering variability on longer time scales because year-to-year changes in tropical Atlantic SST are more strongly modulated by wind-induced latent heat fluxes (*24*, *25*).

The present analysis is an estimate of the direct effect of dust radiative forcing on the upper-ocean heat budget. Our analysis does not exclude other sources of variability in the northern tropical Atlantic (*24*), nor does it account for reductions in atmospheric water vapor (*20*, *26*) or possible increases in cloudiness (*20*, *27*) associated with dust outbreaks. Nor does it include dynamical feedbacks from an atmospheric response to aerosol forcing and associated SST changes, including changes in the latent and sensible heat fluxes (*28*–*30*). Therefore, further analysis of coupled and dynamical feedbacks to aerosol forcing of tropical ocean temperatures is warranted.

Over the past 30 years, temperatures in other tropical ocean basins have been rising steadily, but at a slower rate than in the Atlantic (*31*). At the same time, projections of surface temperature increases under a doubled carbon dioxide climate suggest that the Atlantic should be warming at a rate slower than the other observations (*32*). We suggest that this apparent disconnect between observations and models may be due to the influence of Atlantic dust cover. Our results imply that because dust plays a role in modulating tropical North Atlantic temperature, projections of these temperatures under various global warming scenarios by general circulation models should account for long-term changes in dust loadings. This is especially critical because studies have estimated a reduction in Atlantic dust cover of 40 to 60% under a doubled carbon dioxide climate (*33*), which, on the basis of model runs with an equivalent reduction of the mean dust forcing, could result in an additional 0.3° to 0.4°C warming of the northern tropical Atlantic.

### References and Notes


1. G. R. Foltz, M. J. McPhaden, *Geophys. Res. Lett.* **35**, L20706 (2008).
2. T. P. Barnett *et al*., *Science* **309**, 284 (2005); published online 2 June 2005 (10.1126/science.1112418).
3. B. D. Santer *et al*., *Proc. Natl. Acad. Sci. U.S.A.* **103**, 13905 (2006).
4. M. E. Mann, K. A. Emanuel, *Eos* **87**, 233 (2006).
5. T. L. Delworth, M. E. Mann, *Clim. Dyn.* **16**, 661 (2000).
6. S. B. Goldenberg, C. W. Landsea, A. M. Mestas-Nuñez, W. M. Gray, *Science* **293**, 474 (2001).
7. K. E. Trenberth, D. J. Shea, *Geophys. Res. Lett.* **33**, L12704 (2006).
8. M. Yoshioka *et al*., *J. Clim.* **20**, 1445 (2007).
9. A. T. Evan *et al*., *Geochem. Geophys. Geosyst.* **9**, Q05V04 (2008).
10. R. B. Husar, J. M. Prospero, L. L. Stowe, *J. Geophys. Res.* **102**, 16889 (1997).
11. A. S. Goudie, N. J. Middleton, *Earth Sci. Rev.* **56**, 179 (2001).
12. S. Engelstaedter, I. Tegen, R. Washington, *Earth Sci. Rev.* **79**, 73 (2006).
13. S. Engelstaedter, R. Washington, *Geophys. Res. Lett.* **34**, L15805 (2007).
14. J. M. Prospero, P. J. Lamb, *Science* **302**, 1024 (2003).
15. A. T. Evan, A. K. Heidinger, P. Knippertz, *J. Geophys. Res.* **111**, D12210 (2006).
16. C. Moulin, C. E. Lambert, F. Dulac, U. Dayan, *Nature* **387**, 691 (1997).
17. L. L. Stowe, A. M. Ignatov, R. R. Singh, *J. Geophys. Res.* **102**, 16923 (1997).
18. M. Sato, J. E. Hansen, M. P. Mccormick, J. B. Pollack, *J. Geophys. Res.* **98**, 22987 (1993).
19. C. Deser, M. A. Alexander, M. S. Timlin, *J. Clim.* **16**, 57 (2003).
20. See supporting material on *Science* Online.
21. PATMOS-x data are available at http://cimss.ssec.wisc.edu/patmosx.
22. N. A. Rayner *et al*., *J. Geophys. Res.* **108**, 4407 (2003).
23. All reported significance levels are based on the two-tailed *t* score for the correlation coefficients.
24. G. R. Foltz, M. J. McPhaden, *Geophys. Res. Lett.* **33**, L19703 (2006).
25. G. R. Foltz, M. J. McPhaden, *J. Clim.* **21**, 5048 (2008).
26. J. P. Dunion, C. S. Marron, *J. Clim.* **21**, 5242 (2008).
27. Y. J. Kaufman, I. Koren, L. A. Remer, D. Rosenfeld, Y. Rudich, *Proc. Natl. Acad. Sci. U.S.A.* **102**, 11207 (2005).
28. P. Chang, R. Saravanan, L. Ji, G. C. Hegerl, *J. Clim.* **13**, 2195 (2000).
29. G. R. Foltz, M. J. McPhaden, *J. Clim.* **19**, 6122 (2006).
30. S. Wong, A. E. Dessler, N. M. Mahowald, P. R. Colarco, A. da Silva, *Geophys. Res. Lett.* **35**, L07812 (2008).
31. G. J. Holland, P. J. Webster, *Philos. Trans. R. Soc. London Ser. A* **365**, 2695 (2007).
32. G. A. Vecchi, B. J. Soden, *Nature* **450**, 1066 (2007).
33. N. M. Mahowald, C. Luo, *Geophys. Res. Lett.* **30**, 1903 (2003).



34. We thank three anonymous reviewers for their constructive comments. Supported by grants from NOAA/NESDIS/STAR and Risk Prediction Initiative. The views, opinions, and findings contained in this report are those of the authors and should not be construed as an official NOAA or U.S. government position, policy, or decision.


### Supporting Online Material

www.sciencemag.org/cgi/content/full/1167404/DC1
Materials and Methods
Figs. S1 to S8
References


20 October 2008; accepted 11 March 2009
Published online 26 March 2009;
10.1126/science.1167404
Include this information when citing this paper.


# UV Absorption Cross Sections of ClOOCl Are Consistent with Ozone Degradation Models


**Hsueh-Ying Chen,[1]* Chien-Yu Lien,[1]* Wei-Yen Lin,[1,2] Yuan T. Lee,[1,2] Jim J. Lin[1,3]†**



**Recently, discrepancies in laboratory measurements of chlorine peroxide (ClOOCl) absorption cross sections have cast doubt on the validity of current photochemical models for stratospheric ozone degradation. Whereas previous ClOOCl absorption measurements all suffered from uncertainties due to absorption by impurities, we demonstrate here a method that uses mass-selected detection to circumvent such interference. The cross sections of ClOOCl were determined at two critical wavelengths (351 and 308 nanometers). Our results are sufficient to resolve the controversial issue originating from the ClOOCl laboratory cross sections and suggest that the highest laboratory estimates for atmospheric photolysis rates of ClOOCl, which best explain the field measurements via current chemical models, are reasonable.**


After the discovery of the Antarctic ozone hole (*1*), scientists directed great effort toward studying the underlying chemical and photochemical processes. Until recently, the consensus was that the chemical processes that are responsible for the formation of the ozone hole were reasonably well understood (*2*). However, laboratory data on the ultraviolet absorption spectrum of chlorine peroxide (ClOOCl) published in 2007 by Pope *et al*. (*3*) cast doubt (*4*–*6*) on that understanding. The absorption cross sections measured by Pope *et al*. (*3*) at wavelengths longer than 300 nm ($\lambda > 300$ nm) are much smaller than previously accepted values (*7*). If these recent data are correct, the atmospheric photolysis rates of ClOOCl are much smaller than originally thought, and it would be impossible to produce enough Cl atoms to explain the observed ozone loss via any known chemical mechanisms. Moreover, atmospheric measurements of constituents such as ClO/ClOOCl could not be reconciled with the Pope *et al*. data (*3*), which raises questions (*4*–*6*) about the validity of either the laboratory measurements or model calculations, thus heightening the need for new laboratory studies to either confirm or refute those findings.

Among the major factors controlling ozone loss in the polar stratospheric vortices is the kinetics of the ClOOCl catalytic cycle, in which the photolysis rate of ClOOCl plays a key role (*2*, *5*, *8*). The ultraviolet absorption spectrum of ClOOCl shows a relatively strong and broad feature with a peak at ~245 nm and a long tail extending to 300 nm and longer wavelengths (*3*, *8*–*11*). Because ozone strongly absorbs and therefore depletes sunlight of $\lambda < 300$ nm, it is the


[1]Institute of Atomic and Molecular Sciences, Academia Sinica, Taipei 10617, Taiwan. [2]Department of Chemistry, National Taiwan University, Taipei 10617, Taiwan. [3]Department of Applied Chemistry, National Chiao Tung University, Hsinchu 30010, Taiwan.

*These authors contributed equally to this work.
†To whom correspondence should be addressed. E-mail: jimlin@gate.sinica.edu.tw

weak absorption of ClOOCl at $\lambda > 300$ nm that is responsible for its photodecomposition to Cl atoms. The Cl atoms react with $O_3$ to form $O_2$ + ClO; ClO can then dimerize to form ClOOCl again (*12*), thus catalytically converting $O_3$ to $O_2$. In this atmospherically relevant region of $\lambda > 300$ nm, however, it is difficult to accurately determine the small absorption cross sections of ClOOCl, and there are substantial discrepancies between different laboratory studies. These discrepancies in turn result in large uncertainties in the partitioning of Cl, ClO, and ClOOCl in the resulting ozone loss rate, and therefore in our basic understanding of ozone degradation chemistry.

A review of the literature on both ClOOCl synthesis (*12*–*17*) and its ultraviolet absorption spectrum (*3*, *8*–*11*) reveals that it is extremely difficult to prepare a pure ClOOCl sample at a high enough concentration for an absorption measurement in the gas phase. Except for the latest work by Pope *et al.* (*3*), all other spectroscopic studies (*8*–*11*) largely relied on mass balance to estimate the concentrations of absorbing species. The use of mass balance was based on spectral measurements of the reactants, products, and side products in the synthesis/absorption cell. Accurately estimating the concentrations of absorbing species is further hindered by spectral overlaps, uncertainties in reaction rate constants, and possible unknown side reactions.

Pope *et al.* (*3*) tried to go beyond the method of mass balance by purifying their sample with low-temperature trapping and evaporation. Unfortunately, a pure ClOOCl sample was still unobtainable. The authors then employed a functional fitting method to remove the absorbance of the impurity. They posited that the impurity in their experiments was exclusively $Cl_2$ and that two Gaussian-like functions could represent the ClOOCl spectrum. The relative weighting between the concentrations of $Cl_2$ and ClOOCl was obtained by means of least-squares fitting. This method would work best if the ClOOCl spectrum were very different from the $Cl_2$ spectrum; it becomes unreliable, however, if ClOOCl has a spectral component that is similar to $Cl_2$. Both the mass balance and functional fitting methods are quite complicated, and both have potential weaknesses. Such problems become worse for the long-wavelength region, in which the absorption cross sections of ClOOCl become diminishingly small.

Aware of the impurity problem, we designed an experimental approach in which instead of measuring the attenuation of a photon beam after an absorption cell, we formed a ClOOCl molecular beam and determined the photodissociation probability by measuring the decrease in beam intensity after laser irradiation. Under the condition that the number of photons greatly exceeds the number of molecules, an alternative form of Beer's law can be written as

$$\ln \frac{N_0}{N} = I\sigma\phi \qquad (1)$$

where $N_0$ and $N$ are the numbers of the molecules before and after the laser irradiation, respectively; $I$ is the laser fluence in number of photons per unit area; $\sigma$ is the absorption cross section; and $\phi$ is the dissociation quantum yield. By precisely measuring the ratio of the molecules before and after laser irradiation, we can quantify the absorption cross section without knowing the absolute concentration. We used a mass spectrometer to detect the ClOOCl molecules with high selectivity. In general, this is a powerful method for measuring photodissociation cross sections of species that cannot be prepared in a pure form because the mass selection eliminates interference from most impurities.

Figure 1 shows the schematic setup. The ClOOCl sample is prepared in a pulsed effusive molecular beam and detected downstream with a mass detector at its parent mass. The mass detector (*18*) is equipped with an electron impact ionizer, a quadrupole mass filter, and a Daly-type ion counter. Before the mass detector, the molecular beam is intersected by a pulsed laser beam that photodissociates and thus depletes the ClOOCl molecules with a probability that is proportional to their absorption cross section. Equation 1 could be used to analyze the photodepletion signals and quantify the absorption cross section, but to do so would require knowledge of the absolute fluence distribution of the laser beam, which is difficult to measure precisely. In contrast, comparing the photodepletion signal of ClOOCl to that of a reference molecule only requires the ratio of the laser fluences (which can be more easily measured) to obtain the cross section ratio

$$\frac{[\sigma\phi]_{\mathrm{ClOOCl}}}{[\sigma\phi]_{\mathrm{ref}}} = \frac{I_{\mathrm{ref}}}{I_{\mathrm{ClOOCl}}} \frac{\ln(N/N_0)_{\mathrm{ClOOCl}}}{\ln(N/N_0)_{\mathrm{ref}}} \qquad (2)$$

With a known cross section of the reference molecule, the absolute cross section of ClOOCl can then be obtained.

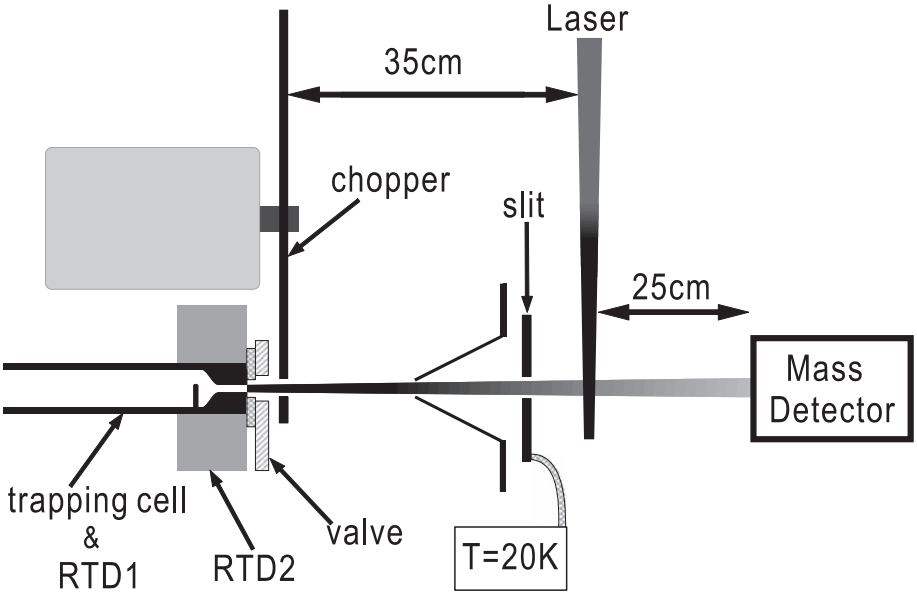


**Fig. 1.** Schematic of the experimental setup (not to scale). The exit of the trapping cell (fused silica) connects to a capillary array (fused silica) that serves as the nozzle of an effusive molecular beam. The temperatures are monitored with resistance temperature detectors (RTD1 and RTD2). The valve (stainless steel and Teflon) isolates the trapping cell from the vacuum chamber during the high pressure period of the ClOOCl condensation.

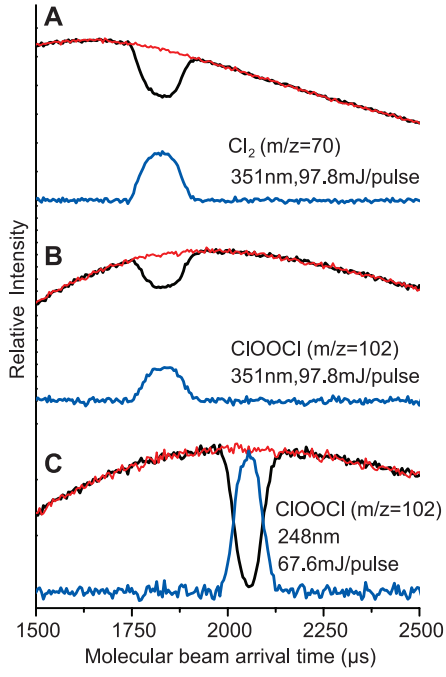


**Fig. 2.** Time profiles of the molecular beams showing the photodepletion of molecules. Black and red lines represent the molecular beam signals with and without laser irradiation, respectively; the blue line is the difference. The laser spot size and delay time are the same in (**A**) and (**B**) but different in (**C**). Therefore, the photo-depletion signal in (C) appears at a different time.

ClOOCl was synthesized by following the method 1 of Pope *et al.* (*3*) ($Cl_2 + h\nu \rightarrow 2Cl$; $Cl + O_3 \rightarrow ClO + O_2$; and $2ClO + M \rightarrow ClOOCl + M$) and trapped in a trapping cell at 150 K. Upon slowly warming up the trap, ClOOCl evaporated and flowed through a temperature-controlled capillary array to form an effusive molecular beam. The thermal velocity distribution of the molecules results in a broad distribution of arrival times for a given species in the molecular beam (Fig. 2).

The mass spectra of the ClOOCl sample in the molecular beam were fully consistent with those previously reported (*14*, *16*). The major impurities were $Cl_2$ and $O_2$; $Cl_2O$ was observed in small amounts. Higher chlorine oxides such as $Cl_2O_3$ were not observed in the mass scans. Additional evidence regarding the ClOOCl sample purity can be found in a very recent work (*19*) that used the same synthesis method and confirmed the purity of the sample by means of both infrared and Raman spectroscopy.

Figure 2, A and B, shows the photodepletion signals of $Cl_2$ and ClOOCl upon 351 nm irradiation at the same laser fluence. At 351 nm, ClOOCl has a photodepletion signal smaller than $Cl_2$, indicating a smaller but still appreciable photodissociation cross section. Figure 2C shows the photodepletion signal of ClOOCl at 248 nm. Because the absorption cross section of ClOOCl at 248 nm is quite large, almost all molecules in the interaction volume have dissociated. For the cross section measurements, saturation effects were carefully checked at various laser fluences. The photodepletion signals of ClOOCl were not affected by different impurity levels at all, even for very large variations (>100 times) of the impurity concentrations.

To determine the absolute cross sections of ClOOCl, we chose $Cl_2$ as the reference molecule at 351 nm and both $Cl_2O$ and $Cl_2$ at 308 nm. The absorption cross sections of these two reference molecules have been well measured (*7*, *20*). It is well known that the excited states of $Cl_2$ are all rapidly dissociative, leading to 100% dissociation ($\phi_{Cl_2} = 1$). A similar argument can be applied to ClOOCl, because ab initio calculations (*21*–*23*) and molecular beam experiments (*24*) all suggest a fast dissociation. The near-ultraviolet photodissociation of $Cl_2O$ has been investigated in a molecular beam (*25*, *26*) and in a gas cell (*27*); the results also indicate a unity dissociation yield under low pressure conditions.

A summary of the cross section measurements is shown in Table 1. A check of consistency was possible at 308 nm because two reference molecules were available. The good agreement of the ClOOCl cross sections determined with two different reference molecules demonstrates the accuracy of this method (*28*). Furthermore, the photodissociation cross section ($\sigma\phi$) is in fact a more relevant quantity than the absorption cross section when estimating the atmospheric photolysis rate (*J* value).

Our results together with previously measured spectra are plotted in Fig. 3. At 308 nm, the value of DeMore *et al.* (*11*) and that recommended by the Jet Propulsion Laboratory (JPL) (*7*) are consistent with ours; Burkholder's value (*9*) is only slightly larger. Because the solar flux of $\lambda < 308$ nm is weak in the stratosphere, the cross section at 351 nm is a much more important factor in the atmospheric photolysis rates of ClOOCl, but previous laboratory data do not agree with each other in this region, as shown in Fig. 3. At 351 nm, the Burkholder cross section is consistent with ours at 200 K but slightly lower than our value at 250 K. Burkholder *et al.* noted only that their data were recorded over the temperature range of 205 to 250 K without mentioning any temperature dependence. Our data show that the temperature dependence of the ClOOCl cross sections at 351 nm is significant. Such temperature dependence may be attributed to the contributions of vibrational hot bands. Because ClOOCl has low-frequency vibrational modes, of which the lowest one is about 127 $cm^{-1}$ (*29*), the populations of vibrational excited states are substantial even at temperatures around 200 K.

Von Hobe *et al.* (*5*, *6*) and others (*2*, *30*) have investigated the effects of using different laboratory values for ClOOCl absorption cross sections in the atmospheric modeling of ozone degradation, and they compared the numerical results with field measurements. Their conclusion is that most observations of ClO, ClOOCl, and ozone loss are best explained by the Burkholder 1990 cross sections (*9*) and that ClOOCl cross sections smaller than the JPL 2006 recommended values (*7*) cannot explain the field observations. Our results clearly indicate that, indeed, those smaller cross sections cannot be correct for $\lambda >$ 300 nm and that even the JPL 2006 recommendation slightly underestimates the cross sections at about 350 nm. The Burkholder cross sections are quite close to our results, suggesting that modeling using those cross sections at wavelengths in the atmospheric window ($\lambda > 300$ nm) should be realistic. The Burkholder cross sections and ours are the largest in the atmospheric window, leading to higher atmospheric photolysis rates of ClOOCl and suggesting the ClOOCl catalytic

**Table 1.** Summary of the measured photodissociation cross sections of ClOOCl.

| Wavelength | Temperature* | Reference molecule (temperature) | $\frac{[\sigma\phi]_{ClOOCl}}{[\sigma\phi]_{ref}}$ | $\sigma_{ref}$ ($10^{-20}$ $cm^2$) | $[\sigma\phi]_{ClOOCl}$ ($10^{-20}$ $cm^2$) |
|---|---|---|---|---|---|
| 351 nm | 200 K | $Cl_2$ (200 K) | 0.608 ± 0.027† | 18.45 | 11.21‡ |
| | 250 K | $Cl_2$ (250 K) | 0.687 ± 0.030 | 18.35 | 12.61 |
| 308 nm | 200 K | $Cl_2O$ (296 K) | 1.116 ± 0.054 | 44.00 | 49.11 |
| | 200 K | $Cl_2$ (250 K) | 2.829 ± 0.132 | 17.30 | 48.95 |
| | 250 K | $Cl_2O$ (296 K) | 1.154 ± 0.060 | 44.00 | 50.77 |
| | 250 K | $Cl_2$ (250 K) | 2.953 ± 0.147 | 17.30 | 51.09 |

*Nozzle temperature of the ClOOCl effusive beam. †See the supporting online material for error analysis. ‡Assuming $\phi_{ref} = 1$.

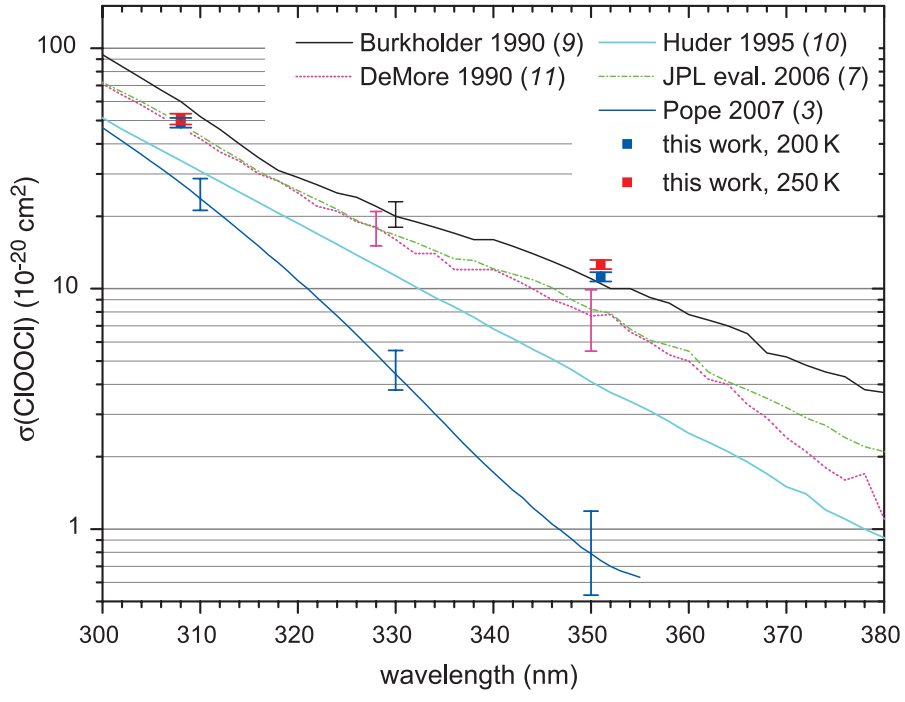


**Fig. 3.** Comparison of different laboratory measurements of absorption cross sections of ClOOCl. Error bars (if available) are also shown at selected wavelengths. The error bars of this work are about the size of the symbols.

cycle is an even more efficient process for polar ozone loss than previously thought (*2*). As for the Pope 2007 cross sections (*3*), it is likely that the authors' functional fitting method may overcorrect for the $Cl_2$ absorbance, resulting in cross sections that are too small in the wavelength region at which $Cl_2$ absorbs significantly (>300 nm).

Although at this point we can only report the cross sections of ClOOCl at two wavelengths because of our requirement of high-intensity lasers, these measurements are surely sufficient to resolve the discrepancies in the photolysis rates of ClOOCl and to restore confidence in standard photochemical models for ozone degradation. We have also demonstrated a promising method for measuring reliable laboratory cross sections of important species in atmospheric chemistry, free from interference by impurities.

### References and Notes


1. J. C. Farman, B. G. Gardiner, J. D. Shanklin, *Nature* **315**, 207 (1985).
2. World Meteorological Organization (WMO), *Scientific Assessment of Ozone Depletion: 2006* (WMO, Geneva, Switzerland, 2007); http://ozone.unep.org/Assessment_Panels/SAP/Scientific_Assessment_2006.
3. F. D. Pope, J. C. Hansen, K. D. Bayes, R. R. Friedl, S. P. Sander, *J. Phys. Chem. A* **111**, 4322 (2007).
4. Q. Schiermeier, *Nature* **449**, 382 (2007).
5. M. von Hobe *et al*., *Atmos. Chem. Phys.* **7**, 3055 (2007).
6. M. von Hobe, *Science* **318**, 1878 (2007).
7. S. P. Sander *et al*., *Chemical Kinetics and Photochemical Data for Use in Atmospheric Studies 06-2* (Jet Propulsion Laboratory, Pasadena, CA, 2006).
8. R. A. Cox, G. D. Hayman, *Nature* **332**, 796 (1988).
9. J. B. Burkholder, J. J. Orlando, C. J. Howard, *J. Phys. Chem.* **94**, 687 (1990).
10. K. J. Huder, W. B. DeMore, *J. Phys. Chem.* **99**, 3905 (1995).
11. W. B. DeMore, E. Tschuikow-Roux, *J. Phys. Chem.* **94**, 5856 (1990).
12. L. T. Molina, M. J. Molina, *J. Phys. Chem.* **91**, 433 (1987).
13. W. J. Bloss, S. L. Nickolaisen, R. J. Salawitch, R. R. Friedl, S. P. Sander, *J. Phys. Chem. A* **105**, 11226 (2001).
14. J. R. McKeachie, M. F. Appel, U. Kirchner, R. N. Schindler, Th. Benter, *J. Phys. Chem. B* **108**, 16786 (2004).
15. J. Plenge *et al*., *J. Phys. Chem. A* **109**, 6730 (2005).
16. T. Ingham, S. P. Sander, R. R. Friedl, *Faraday Discuss.* **130**, 89 (2005).
17. R. Broske, F. Zabel, *J. Phys. Chem. A* **110**, 3280 (2006).
18. J. J. Lin, D. W. Hwang, S. Harich, Y. T. Lee, X. Yang, *Rev. Sci. Instrum.* **69**, 1642 (1998).
19. M. von Hobe, F. Stroh, H. Beckers, T. Benter, H. Willner, *Phys. Chem. Chem. Phys.* **11**, 1571 (2009).
20. C. L. Lin, *J. Chem. Eng. Data* **21**, 411 (1976).
21. A. L. Kaledin, K. Morokuma, *J. Chem. Phys.* **113**, 5750 (2000).
22. A. Toniolo, G. Granucci, S. Inglese, M. Persico, *Phys. Chem. Chem. Phys.* **3**, 4266 (2001).
23. K. A. Peterson, J. S. Francisco, *J. Chem. Phys.* **121**, 2611 (2004).
24. T. A. Moore, M. Okumura, J. W. Seale, T. K. Minton, *J. Phys. Chem. A* **103**, 1691 (1999).
25. R. Aures *et al*., *J. Chem. Phys.* **117**, 2141 (2002).
26. T. A. Moore, M. Okumura, T. K. Minton, *J. Chem. Phys.* **107**, 3337 (1997).
27. S. L. Nickolaisen *et al*., *J. Chem. Phys.* **104**, 2857 (1996).
28. Materials and methods are available as supporting material on *Science* Online.
29. M. Birk *et al*., *J. Chem. Phys.* **91**, 6588 (1989).
30. R. M. Stimpfle, D. M. Wilmouth, R. J. Salawitch, J. G. Anderson, *J. Geophys. Res.* **109**, D03301 (2004).


31. This work is supported by Academia Sinica and National Science Council (NSC 95-2113-M-001-041-MY3), Taiwan. We thank M.-C. Liang for bringing our attention to the ClOOCl issue and K. A. Boering and Y.-P. Lee for valuable comments.


### Supporting Online Material

www.sciencemag.org/cgi/content/full/324/5928/781/DC1
Materials and Methods
Figs. S1 to S3
Table S1
References

23 January 2009; accepted 17 March 2009
10.1126/science.1171305

# Host Inhibition of a Bacterial Virulence Effector Triggers Immunity to Infection

**Vardis Ntoukakis, Tatiana S. Mucyn, Selena Gimenez-Ibanez, Helen C. Chapman, Jose R. Gutierrez, Alexi L. Balmuth, Alexandra M. E. Jones, John P. Rathjen***

**Plant pathogenic bacteria secrete effector proteins that attack the host signaling machinery to suppress immunity. Effectors can be recognized by hosts leading to immunity. One such effector is AvrPtoB of *Pseudomonas syringae*, which degrades host protein kinases, such as tomato Fen, through an E3 ligase domain. Pto kinase, which is highly related to Fen, recognizes AvrPtoB in conjunction with the resistance protein Prf. Here we show that Pto is resistant to AvrPtoB-mediated degradation because it inactivates the E3 ligase domain. AvrPtoB ubiquitinated Fen within the catalytic cleft, leading to its breakdown and loss of the associated Prf protein. Pto avoids this by phosphorylating and inactivating the AvrPtoB E3 domain. Thus, inactivation of a pathogen virulence molecule is one mechanism by which plants resist disease.**

The effector proteins of bacterial, fungal, and oomycete plant pathogens collectively determine pathogenicity on susceptible host species. However, resistance (R) proteins of the plant immune system can recognize these effectors and restrict pathogen growth. The largest class of R proteins is the nucleotide-binding site–plus–leucine-rich repeat (NB-LRR) class (*1*). Recognition of pathogen effectors by R proteins not only protects crops from pathogen attack, but also controls important immune responses in animals (*2*). Despite their importance, R proteins are poorly understood at a mechanistic level. *Pseudomonas syringae* pv. *tomato* DC3000 (*Pst* DC3000) is a pathogen of tomato and *Arabidopsis*, and it injects ~30 effectors into host cells (*3*). One of these effectors, AvrPtoB, degrades host protein kinases through ubiquitination and proteasomal degradation mediated by a C-terminal E3 ubiquitin ligase domain (*4*–*6*). AvrPtoB is widely conserved among diverse bacterial pathogens, including *Xanthomonas*, *Erwinia*, and many strains of *Pseudomonas* (*7*). One target of AvrPtoB is the tomato kinase Fen (*4*), which signals together with the NB-LRR resistance protein Prf. AvrPtoB mutants lacking ubiquitin ligase activity elicit a host immune response mediated by Fen/Prf, leading to defense gene induction and localized cell death known as the hypersensitive response. In resistant cultivars, AvrPtoB is recognized by a protein complex composed of Prf and the Pto kinase, which is highly related (80% identity) to Fen (*8*–*10*). The inability of AvrPtoB to degrade Pto underlies its recognition, but its molecular mechanism is not yet understood.

The Sainsbury Laboratory, Colney, Norwich NR4 7UH, UK.
*To whom correspondence should be addressed. E-mail: john.rathjen@tsl.ac.uk

One important difference between Pto and Fen is their relative kinase activities. Pto autophosphorylation activity in vitro was substantially higher than that of Fen (Fig. 1A), and Pto (but not Fen) was phosphorylated in vivo after transient expression in *Nicotiana benthamiana* leaves (fig. S1) (*11*). Fen was substantially less active than Pto in phosphorylating the in vitro substrate Pti1 (*12*) (fig. S2). While studying interactions between effector protein AvrPtoB and the host kinases, we found that both Pto and Fen were able to phosphorylate AvrPtoB (Fig. 1A). Again Pto was more active, with a Michaelis-Menton constant ($K_m$) of 2.2 μM compared with 10 μM for Fen. A kinase mutant, PtoD164N (*13*), did not autophosphorylate or transphosphorylate AvrPtoB in these assays. We mapped the phosphorylation site on AvrPtoB to $Thr^{450}$ using mass spectrometry analysis, based on the series of y and b ions (Fig. 1B and fig. S3). This residue lies in the E3 ligase domain and is conserved among AvrPtoB homologs from different *P. syringae* strains (*14*).

Protein phosphorylation is important in the regulation of E3 ligases (*15*–*18*). To test the effect of phosphorylation on AvrPtoB E3 ligase activity, we analyzed autoubiquitination in the presence of Pto with the use of recombinant proteins. Increasing amounts of Pto decreased the levels of polyubiquitinated AvrPtoB (Fig. 2A). Similarly, Pto inhibited the trans-ubiquitination of Fen by AvrPtoB in vitro, in a dose-dependent manner (Fig. 2B). Conversely, Fen inhibited its own ubiquitination only when it was allowed to prephosphorylate AvrPtoB (fig. S4), consistent with its weaker kinase activity. Thus, the in vitro data suggest that ubiquitination and phosphorylation are competitive processes that determine the outcome of the AvrPtoB-Pto interaction. Substitution